Disturbance Observer-Based Neural Network Control of a 2-DOF Helicopter System With Input Saturation and Output Constraints

Zhijia Zhao, *Senior Member, IEEE*, Di Zhang, Jiale Wu, Zhijie Liu, *Member, IEEE*, Min Wang, *Member, IEEE*, and Keum-Shik Hong, *Life Fellow, IEEE*

***Abstract*—This article presents a disturbance observer (DO)-based neural network (NN) control for a two-degree-of-freedom (2-DOF) helicopter system with input saturation, external disturbances, and output constraints. First, the uncertainties in the helicopter system are approximated using a radial basis function NN. Subsequently, a DO is used to approximate unknown compound disturbances, involving errors from NN estimation, input saturation, and external disturbances. To address the issue of output constraints imposed at a prescribed time period, a novel time-shift function and an adjusted barrier function are employed. Through the direct Lyapunov method, the boundedness of all control signals in the closed-loop system is verified. Finally, the effectiveness of the proposed control method is validated through numerical simulation results.**

***Index Terms*—Adaptive neural network (NN) control, disturbance observer, input saturation, output constraints, two-degree-of-freedom (2-DOF) helicopter.**

I. Introduction

IN THIS rapidly advancing era of technology, autonomous aerial vehicle (AAV) technology stands as a pivotal component within the modern aviation domain, continually innovating at an unprecedented pace. Helicopters, as a significant type among UAVs, possess traits like lightweight, strong maneuverability [1], and vertical take-off [2] and landing capabilities, empowering them with a diverse range of tasks [3], including disaster relief [4], and the execution of aerial reconnaissance and support missions [2], [5], [6]. However, the helicopter system is a multi-input–multioutput (MIMO) nonlinear system, and its complex dynamic model and interlinked nature among axes restrict its control performance in various environments. Therefore, the development of an effective controller to overcome these challenges is crucial.

To address the aforementioned challenges, researchers have proposed a series of control strategies aimed at achieving stable control of helicopter systems. For instance, Chun et al. [7] devised a Q-learning method to solve the linear quadratic adjustment problem, thereby achieving optimal control of the helicopter system. Maiti et al. [8] introduced a control algorithm based on global stochastic optimization to ensure stable tracking of various desired trajectories by the nonlinear MIMO system. In [9], the Q-learning algorithm was applied to solve the optimal output adjustment problem in helicopter systems, demonstrating the anticipated convergence of the system. It is worth noting that a major limitation of the above studies is that they are based on accurate model conditions of the helicopter system. However, in practical applications, there are uncertainties in the helicopter system model. To ensure that the system can achieve accurate tracking, it is necessary to consider the existence of this uncertainty.

In addressing uncertainties within nonlinear systems, neural networks (NNs) have emerged as pivotal tools owing to their potent parallel computing and excellent generalization capabilities [10], [11], [12], [13]. In the past few years, NNs have attracted widespread attention and achieved important results in multiple fields. For example, Yang and Zheng [14] introduced an NN control that compensated for the dynamic model of a helicopter system, ensuring stable tracking of the system along its intended trajectory. In [15], a broad learning NN control strategy was proposed for a two-degree-of-freedom (2-DOF) helicopter system with actuator failure. In [16], the uncertainties of the helicopter system were estimated through a radial basis function NN (RBFNN)-based adaptive control, enabling rapid convergence of system errors within a finite time. Zou et al. [17] developed a control methodology amalgamating NNs with sliding mode control, enhancing the

Received 3 September 2024; accepted 27 January 2025. Date of publication 24 February 2025; date of current version 17 April 2025. This work was supported in part by the National Natural Science Foundation of China under Grant 62273112, Grant 62273156, Grant 62433011, Grant 62473039, and Grant U24A20329; in part by the Guangdong Basic and Applied Basic Research Foundation under Grant 2023B1515120018 and Grant 2023B1515120019; in part by the Beijing Nova Program under Grant 20240484561; in part by the Joint Fund of Ministry of Education for Equipment Pre-Research under Grant 8091B03032303; and in part by the National Research Foundation of Korea Funded by the Ministry of Science and ICT, South Korea, under Grant IRIS-2023-00207954. This article was recommended by Associate Editor Y.-P. Huang. *(Corresponding author: Zhijie Liu.)*

Zhijia Zhao, Di Zhang, and Jiale Wu are with the School of Mechanical and Electrical Engineering, Guangzhou University, Guangzhou 510006, China (e-mail: zhjzhaoscut@163.com; 2112307044@e.gzhu.edu.cn; 2112107005@e.gzhu.edu.cn).

Zhijie Liu is with the School of Intelligence Science and Technology, University of Science and Technology Beijing, Beijing 100083, China (e-mail: liuzhijie@ustb.edu.cn).

Min Wang is with the School of Automation Science and Engineering, South China University of Technology, Guangzhou 510641, China (e-mail: auwangmin@scut.edu.cn).

Keum-Shik Hong is with the School of Mechanical Engineering, Pusan National University, Busan 46241, South Korea (e-mail: kshong@pusan.ac.kr).

Color versions of one or more figures in this article are available at https://doi.org/10.1109/TSMC.2025.3538990.

Digital Object Identifier 10.1109/TSMC.2025.3538990

control performance of a 2-DOF helicopter system. The aforementioned studies concentrated on addressing the uncertainty issue within helicopter systems and have shown significant advancements in this area. However, in the real world, many practical systems and devices often encounter input saturation, which severely restricts system performance and may even lead to system instability. This prompts us to conduct further research on input saturation.

In practical engineering, due to the physical limitations of actuators, system input signals are invariably bound by upper limits [18], [19], leading to unavoidable input saturation. In order to overcome the saturation effect in nonlinear systems, researchers have developed a variety of methods. For example, Song et al. [20] proposed an adaptive tracking control for nonlinear systems with compound problems of input saturation and unknown dynamics. In [21], efficient tracking performance of rigid manipulator joints amidst input torque saturation scenarios was guaranteed by an NN control. Sun et al. [22] designed a fixed-time control strategy that used an auxiliary system to compensate for the effects of input saturation, achieving stable and rapid convergence of system errors. Lv et al. [23] introduced an adaptive dynamic surface control strategy to deal with the input saturation, ensuring that tracking error asymptotically convergence to zero. However, it should be emphasized that the studies mentioned exclusively concentrated on addressing the problem of input saturation in nonlinear systems, overlooking the impact of external disturbances on the system. In the field of helicopters, the system may be disturbed by external environmental factors, thereby degrading the performance of the closed-loop system. Therefore, a comprehensive consideration of external disturbances affecting the system is crucial to accurately reflect the actual conditions of helicopter operation.

The disturbance observer (DO) can estimate unknown external disturbances within the system, thereby compensating for these disturbances and ensuring the stability and reliability of system performance [24]. In recent years, there has been a dedicated effort toward designing DO, resulting in the development of various control schemes based on DO. For example, Zhang and He [25] designed a piecewise switching nonlinear DO for eliminating the effects of system uncertainty and unknown disturbances. In [26], by introducing an NN control strategy with a discrete-time DO, uncertainties and unknown disturbances within UAV systems were addressed. In [27], an adaptive control strategy combining observers and sliding mode functions was proposed for systems facing the compound challenge of time-varying disturbances and actuator failures. Zhang et al. [28] proposed an output feedback control algorithm that mitigates the adverse effects of bounded disturbances through a DO, significantly enhancing the robustness of the system. Although the above-mentioned studies on DO have made significant achievements, the output constraints of the helicopter systems are overlooked. In actual application, the helicopter may be limited by the external environment during operation, leading to constraints on the system output and consequently impacting its stability and performance. Therefore, the impact of output constraints should be considered in controller design.

For the past few years, a wide variety of scholars have developed various control methods to address the issue of output constraints. For example, Ni and Shi [29] devised an adaptive NN control strategy, integrating an integral barrier Lyapunov function (BLF) to resolve output constraint, ultimately achieving globally stable control for nonlinear systems. In [30], a self-triggered control approach was tailored for uncertain nonlinear systems featuring output constraints. In [31], barrier function analysis technology was applied to propose an adaptive NN control strategy aimed at resolving the trajectory tracking issue of the system. In addition, Yan et al. [32] devised a control barrier function to address output constraints in unknown multiagent systems, ensuring the safety of system operations. In [33], an asymmetric time-varying BLF (ATVBLF) was introduced, and an adaptive NN control method was proposed to address the tracking control problem for a class of uncertain nonlinear strict-feedback systems with time-varying full-state constraints. Farzan et al. [34] proposed a control method based on control Lyapunov functions and barrier functions to ensure stable and safe operation of robots under output constraint boundaries. It can be observed that the aforementioned studies primarily focus on exploring output constraints within an infinite time range ($t\geq 0$). However, in practical applications, it is essential to consider output constraints imposed at a prescribed time period (OCIPT). This means that constraints can be imposed on the system during a certain period of time, and it remains unconstrained during other periods. An intuitive example would be a helicopter starting in open space, navigating through a tunnel, and then emerging into another open space. This sequence involves the system transitioning from an unconstrained state to a constrained one and then back to an unconstrained state. This situation motivates us to delve further into our research. In addition, as far as we know, although significant advancements have been achieved in studying output constraints, external disturbances, and input saturation in individual facets of nonlinear systems, research addressing the composite issue of concurrent output constraints, external disturbances, and input saturation within a 2-DOF helicopter system remains relatively scarce. This has motivated us to conduct this research. Inspired by the previous discussions, we aim to investigate an adaptive NN control strategy for achieving trajectory tracking control in a 2-DOF helicopter system with output constraints, external disturbances, and input saturation. The primary contributions of this study can be summarized as follows.

1) Differing from [25], [26], and [27], this study introduces a DO to address the adverse effects caused by an unknown compound disturbance, encompassing errors during NN approximation, errors due to input saturation, and external disturbances. This method enhances the robustness of the system.
2) Unlike the output constraints in [29], [30], and [31], this study proposes a control strategy that employs a new time-shift function and an adjusted barrier function. This method addresses the OCIPT issue and ensures stable tracking performance of the system. Furthermore, the proposed control strategy can handle scenarios with

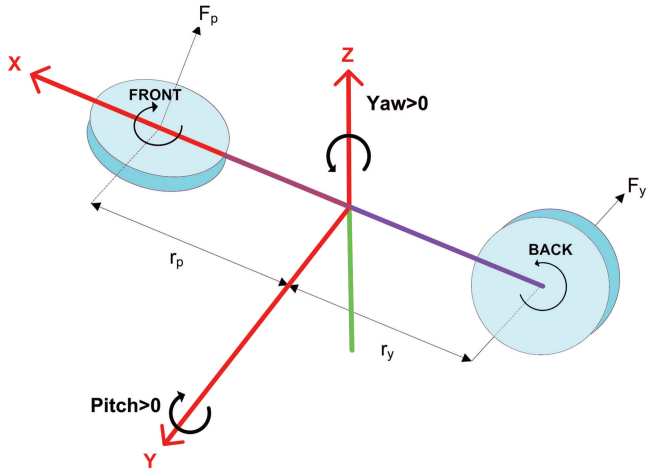

Fig. 1. Model of a 2-DOF helicopter.

no output constraints or continuous output constraints without requiring modifications to the control structure, thereby enhancing its versatility.

3) Dissimilar to [20], [28], and [29], this study proposes an adaptive NN control based on DO, effectively addressing the interplay among input saturation, external disturbances, and output constraints. Moreover, rigorous Lyapunov stability analysis validates the boundedness of the closed-loop system.

II. Problem and Preliminary Formulation

A. Problem Formulation

The model of a 2-DOF helicopter is displayed in Fig. 1. The helicopter is designed with dual propellers. A horizontally positioned rotor generates a force, denoted as F_p, at a distance r_p from the midpoint of the helicopter, serving to control pitch. Concurrently, a vertically positioned rotor produces a force, denoted as F_p, at a distance r_y from the midpoint of the helicopter, utilized for yaw operation.

According to [35], using the Lagrange formula allows for the description of the system's dynamical equation as

$$\left(T_{pp}+m_v l_a^2\right)\ddot{\Theta} = L_{ff}V_{pp}+L_{fd}V_{yy}-m_v g_v l_a\cos(\Theta) - D_{pp}\dot{\Theta}-m_v l_a^2\dot{\Psi}^2\cos(\Theta)\sin(\Theta) \tag{1}$$

$$\left(T_{yy}+m_v l_a^2\cos^2(\Theta)\right)\ddot{\Psi} = L_{df}V_{pp}+L_{dd}V_{yy}-D_{yy}\dot{\Psi} + 2m_v l_a^2\dot{\Theta}\dot{\Psi}\cos(\Theta)\sin(\Theta) \tag{2}$$

where Ψ and Θ are the yaw and pitch angles, respectively, l_a is the distance from the origin of the body-fixed frame to the action point, m_v is the mass of the helicopter, g_v is the gravitational constant, L_{ff}, L_{fd}, L_{df}, and L_{dd} denote the thrust torque constants, D_{yy} and D_{pp} denote the viscous damping of the yaw and pitch axes, respectively, and T_{yy} and T_{pp} represent the moments of inertia of the rotating beam around the yaw and pitch axes, respectively.

Define the state variable $x=[x_1,x_2]^T$, where $x_1=[\Theta,\Psi]^T$ and $x_2=[\dot{\Theta},\dot{\Psi}]^T$. Considering the comprehensive challenges of internal uncertainties within the system, input saturation, and external disturbances, we transform (1) and (2) into the following state-space equations:

$$\dot{x}_1 = x_2 \tag{3}$$

$$\dot{x}_2 = B(x_1,x_2)+\Delta B(x_1,x_2) + (N(x_1,x_2)+\Delta N(x_1,x_2))S(u)+d(t) \tag{4}$$

$$y = x_1 \tag{5}$$

where $\Delta B(x_1,x_2)$ and $\Delta N(x_1,x_2)$ represent the internal uncertainties within the system, and $B(x_1,x_2)$ and $N(x_1,x_2)$ are given as follows:

$$B(x_1,x_2) = \begin{bmatrix} \frac{-m_v g_v l_a\cos(\Theta)-D_{pp}\dot{\Theta}-m_v l_a^2\dot{\Psi}^2\sin(\Theta)\cos(\Psi)}{T_{pp}+m_v l_a^2} \\ \frac{-D_{yy}\dot{\Psi}+2m_v l_a^2\dot{\Psi}\dot{\Theta}\sin(\Theta)\cos(\Theta)}{T_{yy}+m_v l_a^2\cos^2(\Theta)} \end{bmatrix} \tag{6}$$

$$N(x_1,x_2) = \begin{bmatrix} \frac{L_{ff}}{T_{pp}+m_v l_a^2} & \frac{L_{fd}}{T_{pp}+m_v l_a^2} \\ \frac{L_{df}}{T_{yy}+m_v l_a^2\cos^2(\Theta)} & \frac{L_{dd}}{T_{yy}+m_v l_a^2\cos^2(\Theta)} \end{bmatrix}. \tag{7}$$

Furthermore, $d(t)$ is the external disturbance, y is the system output, u is the system control input, and $S(u)=[V_{pp},V_{yy}]^T$ denotes the output of saturation nonlinearity, which is described as follows [36]:

$$S(u)=\text{sat}(u)=\begin{cases} u_{\max}, & \text{if} \quad u>u_{\max} \\ u, & \text{if} \quad u_{\min}\le u\le u_{\max} \\ u_{\min}, & \text{if} \quad u<u_{\min} \end{cases} \tag{8}$$

where $u_{\max}>0$ and $u_{\min}<0$ are the upper and lower bounds of the saturation, respectively. Obviously, the designed nominal input u can occasionally exceed the actually provided actual input $S(u)$. Therefore, there exists a bounded difference between the nominal and actual control inputs [37]

$$\delta(u)=S(u)-u. \tag{9}$$

Substituting (9) into (4) yields

$$\begin{aligned}\dot{x}_2 &= B(x_1,x_2)+\Delta B(x_1,x_2)+N(x_1,x_2)(\delta(u)+u) \\ &\quad +\Delta N(x_1,x_2)(\delta(u)+u)+d(t) \\ &= B(x_1,x_2)+N(x_1,x_2)(\delta(u)+u)+d(t)+P(x,u)\end{aligned} \tag{10}$$

where $P(x,u)=\Delta B(x_1,x_2)+\Delta N(x_1,x_2)(\delta(u)+u)$.

To facilitate the acceptance of a viable solution within the system in consideration, the following lemmas and assumptions are made.

Lemma 1 [38]: Due to its strong capacity for generalization and adaptation within dynamic environments, RBFNNs are frequently employed to handle uncertainties in nonlinear systems. Then, the following RBFNN to approximate the continuous and unknown function J_n: $\mathbb{R}^i\to\mathbb{R}$:

$$J_n(X)=W^T H(X) \tag{11}$$

where the input vector $X\in\mathbb{R}^i$, weight vector $W=[w_1,w_2,\ldots,w_j]^T\in\mathbb{R}^j$, with $j>1$ being the number of NN nodes, and basis function vector $H(X)=$

$[h_1(X), h_2(X), \ldots, h_j(X)]^T$, with h_q being chosen as the Gaussian function in the following form:

$$h_q(X) = \exp\left[\frac{-(X-h_q)^T(X-h_q)}{\iota_q^2}\right] \tag{12}$$

where $h_q = [h_{q1}, h_{q2}, \ldots, h_{qi}]^T$ and ι_q are the center of the receptive field and the width of the Gaussian function, respectively.

Based on (12), a suitable node selection enables RBFNNs to effectively approximate any continuous function $J(X)$ as follows:

$$J(X) = W^{*T}H(X) + \eta(X) \tag{13}$$

where W^* represents the optimal weight matrix, and $\eta(X)$ denotes the approximation error and satisfying $\|\eta(X)\| \leq \bar{\eta}$, with $\bar{\eta}$ being an unknown constant. The optimal weight matrix of RBFNN is given by

$$W^* = \arg\min_{W\in\mathbb{R}^j}\left\{\sup_{X\in\Omega_X}\left|J(X) - W^TH(X)\right|\right\}. \tag{14}$$

Lemma 2 [39]: For a positive definite and continuous candidate Lyapunov function, if it remains bounded at the initial condition $V(0)$ and the following equation holds:

$$\dot{V}(x) \leq -aV(x) + C \tag{15}$$

where $a > 0$, C are constants, then $V(x)$ is bounded.

Assumption 1 [40]: For all $t > 0$, the desired trajectory x_d is a sufficiently smooth function, and x_d, $\dot{x}_d$, and $\ddot{x}_d$ are known, continuous, and bounded. Also, there exist constants $\underline{x}_d$ and $\bar{x}_d$ such that $\underline{x}_d < x_d < \bar{x}_d$.

Assumption 2 [41]: The control gain matrix $N(x_1, x_2)$ is bounded and invertible, and there exists an unknown constant $\bar{N}$ satisfying $0 < \|N(x_1, x_2)\| \leq \bar{N}$.

Assumption 3 [42]: The external disturbance $d(t)$ is assumed to be continuous and possess finite energy, and there exist unknown constants $\bar{d} > 0$ and $\bar{d}_1 > 0$ such that $\|d(t)\| \leq \bar{d}$ and $\|\dot{d}(t)\| \leq \bar{d}_1$.

B. Time-Shift Function

The OCIPT includes three phases: 1) unrestricted; 2) constrained; and 3) back to unrestricted. The key is to ensure that the constraints are effective only within the prescribed time range (T_x and T_y) and to guarantee a smooth transition of the controller between the unrestricted and constrained phases. To address this challenge, the following time-shift function is proposed:

$$\omega_l(t) = \begin{cases} e^{-\frac{\left(\tan\left(\frac{\pi(T_x-t)}{2T_x}\right)\right)^{2m}}{2\mu_1^{2m}}}, & 0 \leq t < T_x \\ 1, & T_x \leq t < T_y \\ e^{-\frac{(t-T_y)^{2m}}{2\mu_2^{2m}}}, & t \geq T_y \end{cases} \tag{16}$$

for $l = 1, 2$, where m is the order of the system, and μ_1 and μ_2 are positive constants.

Invoking (16), we have the following properties.

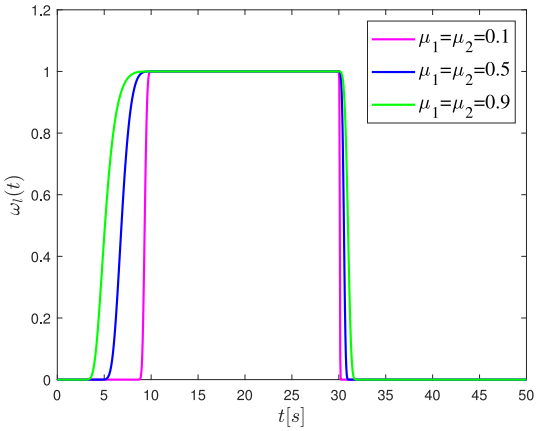

Fig. 2. Variations in ω_l with $T_x = 10$ s and $T_y = 30$ s.

1) ω_l is monotonically increasing with time for $0 \leq t < T_x$, and when $t \to T_x^-$, $\omega_l(T_x^-) = 1$;
2) $\omega_l = 1$ always holds for $T_x \leq t < T_y$;
3) $\omega_l(t)$ with $\omega_l(T_y) = 1$ is monotonically decreasing with time for $t \geq T_x$, and when $t \to \infty$, $\omega_l \to 0$;
4) the time derivative of ω_l is continuous for $t \geq 0$.

Define the tracking error as $z_1 = x_1 - x_d$, with $x_d = [\Theta_d, \Psi_d]^T$ being a desired tracking trajectory. Then, we introduce the following auxiliary variable:

$$\vartheta_l(t) = \begin{cases} \omega_l z_{1l}, & 0 \leq t < T_x \\ z_{1l}, & T_x \leq t < T_y \\ \omega_l z_{1l}, & t \geq T_y \end{cases} \tag{17}$$

where $\vartheta_l = [\vartheta_1, \vartheta_2]^T \in \mathbb{R}^2$ and $\omega_l = [\omega_1, \omega_2]^T \in \mathbb{R}^2$. Through the transformation of (17), it can be deduced that when $0 < t < T_x$ and $t > T_y$, since $\omega_l \to 0$, it ruselts in the auxiliary variable $\vartheta_l \to 0$.

Remark 1: Fig. 2 illustrates the variations in ω_l under different values of μ_1 and μ_2. For $0 \leq t < T_x$, the parameter μ_1 determines the rate at which ω_l approaches 1. A higher μ_1 results in a slower ascent of ω_l toward 1. As for $t \geq T_y$, it is μ_2 that governs the speed of ω_l convergence toward 0. A larger μ_2 leads to a slower convergence of ω_l toward 0. Therefore, smaller values of μ_1 and μ_2 facilitate a swift transition of ω_l between nonzero and zero.

Remark 2: Based on the properties of ω_l, we understand that when $\omega_l = 1$, the system is in a constrained state; when $\omega_l = 0$, the system is in an unconstrained state. Therefore, by setting $T_x = 0$ and $T_y > 0$, constraints can be imposed during the initial time period $(0 - T_x)$. When $T_x > 0$ and $T_y > 0$, constraints can be applied after the system starts (from T_x to T_y). Moreover, setting $T_x = 0$ and $T_y = 0$ ensures no constraints are imposed on the system for all $t \geq 0$.

C. Barrier Function

Due to inherent deficiencies in the definition of traditional BLF-based control methods during the unconstrained phase, they are unable to effectively address the OCIPT problem. To handle this issue and simultaneously deal with unconstrained

and prescribed time constraints within a comprehensive framework, the following barrier function is proposed:

$$\xi_l = \frac{Q_{fl}Q_{gl}z_{1l}}{(Q_{gl}+\vartheta_l)(Q_{fl}-\vartheta_l)}, l = 1, 2 \tag{18}$$

where Q_{fl} and Q_{gl} are time-varying functions representing the upper and lower boundaries of output constraints, respectively. It is shown from (18) that if the initial condition $-Q_{fl}(0) < \vartheta_l(0) < Q_{gl}(0)$ is satisfied, then for all $t \geq 0$, ξ_j remains well defined. In addition, ξ_l tends to infinity if and only if ϑ_l approaches either $-Q_{gl}$ or Q_{fl}. Therefore, proving the boundedness of ξ_l for all $t \geq 0$ ensures $-Q_{fl} < \vartheta_l < Q_{gl}$.

Remark 3: From the expressions of (17) and (18), it can be deduced that $\xi_l \to \infty$ if and only if $z_{1l} \to -(Q_{gl}/\omega_l)$ or $z_{1l} \to (Q_{fl}/\omega_l)$. According to Remark 1, for $0 \leq t < T_x$ and $t \geq T_y$, $\omega_l \to 0^+$. Consequently, we derive that $-\infty < z_{1l} < +\infty$. By combining $z_1 = x_1 - x_d$, we conclude that $-\infty < x_{1l} - x_{dl} < +\infty$, which implies that $-\infty + \underline{x}_{dl} < x_{1l} < +\infty + \bar{x}_{dl}$. Therefore, the system state variable x_1 is unconstrained for $0 \leq t < T_x$ and $t \geq T_y$. Similarly, from (16), it is observed that $\omega_l = 1$ for $T_x < t < T_y$, which means that $-Q_{gl} < z_{1l} < Q_{fl}$. Consequently, we derive that $-Q_{gl} + \underline{x}_{dl} < x_{1l} < Q_{fl} + \bar{x}_{dl}$. By defining $E_{Gl} = -Q_{gl} + \underline{x}_{dl}$ and $E_{Fl} = Q_{fl} + \bar{x}_{dl}$, we establish $E_{Gl} < x_{1l} < E_{Fl}$. Therefore, the system state variable x_1 is constrained for $T_x < t < T_y$, with E_{Fl} as the upper bound and E_{Gl} as the lower bound. Based on the preceding analysis, the OCIPT is achievable.

III. Control Design

From (10), it is observed that due to the uncertainties in $P(x, u)$, model-based control design may not be feasible. To address these issues, we employ the RBFNN from Lemma 1 to approximate the uncertainties and enhance system performance through online estimation. Therefore, the following is derived:

$$M_D P(x, u) = W^{*T} H(X) + \eta(X) \tag{19}$$

where $M_D = M_D^T \in \mathbb{R}^{2\times 2}$ represents the design matrix of the DO, W^* denotes the optimal weight matrix, and $X = [x_1^T, x_2^T, x_d^T, \dot{x}_d^T]^T$ represents the input vector. $\eta(X)$ is the approximation error that satisfies $\|\eta(X)\| \leq \bar{\eta}$, when $\bar{\eta}$ is an unknown positive constant.

Substituting (19) into (10) yields

$$\begin{aligned}\dot{x}_2 = {} & B + Nu + N\delta(u) + M_D^{-1} W^{*T} H(X) \\ & + M_D^{-1}\eta(X) + d(t).\end{aligned} \tag{20}$$

We establish the following compounded function of disturbances:

$$D(t) = N\delta(u) + M_D^{-1}\eta(X) + d(t). \tag{21}$$

Based on the bounded properties of both $\delta(u)$ and $\eta(X)$, along with Assumption 3, we can derive that $\|\dot{D}(t)\| \leq \bar{D}(t)$ [43]. Then, we rewrite (20) as

$$\dot{x}_2 = B + Nu + M_D^{-1} W^{*T} H(X) + D(t). \tag{22}$$

Define the error variable of the system as

$$e_2 = x_2 - \alpha \tag{23}$$

where α represents a virtual control variable.

Substituting (22) into $\dot{e}_2$ results in

$$\dot{e}_2 = B + Nu + M_D^{-1} W^{*T} H(X) + D - \dot{\alpha}. \tag{24}$$

A. Design and Analysis of Nonlinear Disturbance Observer

To approximate the unknown variable $D(t)$, we devise the following nonlinear DO:

$$\hat{D} = \varrho + M_D x_2 \tag{25}$$

$$\dot{\varrho} = -M_D\left(B + Nu + \hat{D}\right) - \hat{W}^T H(X) + e_2 \tag{26}$$

where ϱ is an auxiliary function.

Considering (25) and (26), we obtain

$$\begin{aligned}\dot{\hat{D}} &= \dot{\varrho} + M_D \dot{x}_2 \\ &= M_D\left(D - \hat{D}\right) + W^{*T} H(X) - \hat{W}^T H(X) + e_2.\end{aligned} \tag{27}$$

Defining $\tilde{W} = \hat{W} - W^*$ and $\tilde{D} = D - \hat{D}$, and considering (27), we have

$$\dot{\tilde{D}} = \dot{D} - \dot{\hat{D}} = \dot{D} - M_D\tilde{D} + \tilde{W}^T H(X) - e_2. \tag{28}$$

Invoking (28), we obtain

$$\tilde{D}^T\dot{\tilde{D}} = \tilde{D}^T\tilde{W}^T H(X) + \tilde{D}^T\dot{D} - \tilde{D}^T M_D\tilde{D} - \tilde{D}^T e_2. \tag{29}$$

Taking into account the following inequalities gives:

$$\tilde{D}^T\dot{D} \leq \frac{1}{2}\tilde{D}^T\tilde{D} + \frac{1}{2}\|\dot{D}\|^2 \leq \frac{1}{2}\tilde{D}^T\tilde{D} + \frac{1}{2}\bar{D}^2 \tag{30}$$

$$\tilde{D}^T\tilde{W}^T H(X) \leq 0.5\Xi\Upsilon^2\|\tilde{D}\|^2 + \frac{1}{2\Xi}\|\tilde{W}\|^2 \tag{31}$$

where $\|H(X)\| \leq \Upsilon$, and $\Xi > 0$ is a design parameter.

According to the inequalities (30) and (31), then (29) can be rewritten as

$$\begin{aligned}\tilde{D}^T\dot{\tilde{D}} &\leq \frac{1}{2}\tilde{D}^T\tilde{D} + \frac{1}{2}\bar{D}^2 - \tilde{D}^T M_D\tilde{D} + \frac{1}{2\Xi}\|\tilde{W}\|^2 \\ &\quad + 0.5\Xi\Upsilon^2\|\tilde{D}\|^2 - \tilde{D}^T e_2 \\ &= -\tilde{D}^T\left[M_D - \left(\frac{1}{2} + 0.5\Xi\Upsilon^2\right)I_{2\times 2}\right]\tilde{D} \\ &\quad + \frac{1}{2\Xi}\|\tilde{W}\|^2 + \frac{1}{2}\bar{D}^2 - \tilde{D}^T e_2.\end{aligned} \tag{32}$$

B. Design and Stability Analysis of Adaptive Neural Network Control

Before embarking on the design of adaptive NN control, we take the derivative of the barrier function ξ_l

$$\dot{\xi}_l = \beta_l\dot{z}_{1l} + \varepsilon_l\dot{\omega}_l - \psi_l\dot{Q}_{fl} + \gamma_l\dot{Q}_{gl} \tag{33}$$

where $\beta_l = [Q_{gl}Q_{fl}(Q_{gl}Q_{fl} + \vartheta_l^2)/(Q_{gl} + \vartheta_l)^2(Q_{fl} - \vartheta_l)^2]$, $\varepsilon_l = -[Q_{gl}Q_{fl}z_{1l}^2(Q_{fl} - Q_{gl} - 2\vartheta_l)/(Q_{gl} + \vartheta_l)^2(Q_{fl} - \vartheta_l)^2]$, $\psi_l = [Q_{gl}\vartheta_l z_{1l}(Q_{gl} + \vartheta_l)/(Q_{gl} + \vartheta_l)^2(Q_{fl} - \vartheta_l)^2]$, and $\gamma_l = [Q_{fl}\vartheta_l z_{1l}(Q_{fl} - \vartheta_l)/(Q_{gl} + \vartheta_l)^2(Q_{fl} - \vartheta_l)^2]$ $l = 1, 2$.

Let $\xi = [\xi_1, \xi_2]^T \in \mathbb{R}^2$, $\omega = [\omega_1, \omega_2]^T \in \mathbb{R}^2$, $Q_f = [Q_{f1}, Q_{f2}]^T \in \mathbb{R}^2$, $Q_g = [Q_{g1}, Q_{g2}]^T \in \mathbb{R}^2$, $\beta = \text{diag}[\beta_1, \beta_2] \in \mathbb{R}^{2\times 2}$, $\varepsilon = \text{diag}[\varepsilon_1, \varepsilon_2] \in \mathbb{R}^{2\times 2}$, $\psi = \text{diag}[\psi_1, \psi_2] \in \mathbb{R}^{2\times 2}$, and $\gamma = \text{diag}[\gamma_1, \gamma_2] \in \mathbb{R}^{2\times 2}$.

Note that $z_1 = x_1 - x_d$ and (3), the derivative of z_1 is expressed as

$$\dot{z}_1 = x_2 - \dot{x}_d. \tag{34}$$

Now, the coordinate transformation is defined as $e_1 = \xi$. According to (23), (33), and (34), the derivative of e_1 is derived as follows:

$$\dot{e}_1 = \beta(e_2 + \alpha - \dot{x}_d) + \varepsilon\dot{\omega} - \psi\dot{Q}_f + \gamma\dot{Q}_g. \tag{35}$$

The Lyapunov function V_1 is chosen as follows:

$$V_1 = \frac{1}{2}e_1^T e_1. \tag{36}$$

Deriving its time derivative yields

$$\begin{aligned}\dot{V}_1 &= e_1^T\dot{e}_1 \\ &= e_1^T\beta(e_2 + \alpha - \dot{x}_d) + e_1^T\left(\varepsilon\dot{\omega} - \psi\dot{Q}_f + \gamma\dot{Q}_g\right).\end{aligned} \tag{37}$$

The virtual control variable is designed as

$$\alpha = -\beta^{-1}\left(k_1 e_1 + \varepsilon\dot{\omega} - \psi\dot{Q}_f + \gamma\dot{Q}_g\right) + \dot{x}_d \tag{38}$$

where k_1 is a design positive parameter.

Substituting (38) into (37) yields

$$\dot{V}_1 = -e_1^T k_1 e_1 + e_1^T\beta e_2. \tag{39}$$

From (38), it can be observed that a repeated differentiating α results in an explosion of complexity problem. To address this challenge, we utilize the dynamic surface control technology. Introducing a first-order filter α_M and allowing α to pass through it [44], we then derive

$$\tau\dot{\alpha}_M + \alpha_M = \alpha, \quad \alpha_M(0) = \alpha(0) \tag{40}$$

where τ denotes the time constant of the filter.

By defining the surface error as $\rho = \alpha_M - \alpha$, we obtain

$$\begin{aligned}\dot{\rho} &= \dot{\alpha}_M - \dot{\alpha} \\ &= -\frac{\rho}{\tau} + \left(-\frac{\partial\alpha}{\partial x_1}\dot{x}_1 - \frac{\partial\alpha}{\partial x_d}\dot{x}_d - \frac{\partial\alpha}{\partial\dot{x}_d}\ddot{x}_d - \frac{\partial\alpha}{\partial\omega}\dot{\omega} - \frac{\partial\alpha}{\partial\dot{\omega}}\ddot{\omega}\right. \\ &\quad \left. - \frac{\partial\alpha}{\partial Q_f}\dot{Q}_f - \frac{\partial\alpha}{\partial\dot{Q}_f}\ddot{Q}_f - \frac{\partial\alpha}{\partial Q_g}\dot{Q}_g - \frac{\partial\alpha}{\partial\dot{Q}_g}\ddot{Q}_g\right) \\ &= -\frac{\rho}{\tau} + Y\left(x_1, x_d, \dot{x}_d, \dot{\omega}, Q_f, \dot{Q}_f, Q_g, \dot{Q}_g\right)\end{aligned} \tag{41}$$

where $Y(\cdot)$ represents a continuous function related to $\Omega(\cdot)$. As the set $\Omega(\cdot)$ is compact, there exists a maximum value $\bar{Y}$ within the set $\Omega(\cdot)$, such that $\|Y\| \le \bar{Y}$.

Then, (41) can be rewritten as

$$\dot{\rho} \le -\frac{\rho}{\tau} + \bar{Y}. \tag{42}$$

We select the candidate Lyapunov function V_2 as

$$V_2 = V_1 + \frac{1}{2}e_2^T e_2. \tag{43}$$

Its time derivative can be derived as

$$\begin{aligned}\dot{V}_2 &= \dot{V}_1 + e_2^T\dot{e}_2 \\ &= -e_1^T k_1 e_1 + e_1^T\beta e_2 + e_2^T\left[B + Nu + M_D^{-1}W^{*T}H(X)\right] \\ &\quad + e_2^T D - e_2^T\dot{\alpha}.\end{aligned} \tag{44}$$

The adaptive NN control law is proposed as

$$u = N^{-1}\left[-B - M_D^{-1}\hat{W}^T H(X) - \rho^T\beta - \hat{D} + \dot{\alpha}_M - k_2 e_2\right] \tag{45}$$

with k_2 being a design positive parameter.

The updating law of $\hat{W}$ is designed as

$$\dot{\hat{W}} = \Lambda_W\left[H(X)e_2^T M_D^{-1} - \sigma_W\hat{W}\right] \tag{46}$$

where Λ_W represents a constant gain matrix, and σ_W denotes a small positive constant.

Substituting (45) into (44) yields

$$\begin{aligned}\dot{V}_2 &= -e_1^T k_1 e_1 - e_2^T k_2 e_2 - e_2^T M_D^{-1}\tilde{W}^T H(X) \\ &\quad + e_2^T\tilde{D} + e_2^T\left(-\frac{\rho}{\tau} + Y\right).\end{aligned} \tag{47}$$

The candidate Lyapunov function is defined as follows:

$$V_3 = V_2 + \mathrm{tr}\left\{\frac{1}{2}\tilde{W}^T\Lambda_W^{-1}\tilde{W}\right\} + \frac{1}{2}\tilde{D}^T\tilde{D} + \frac{1}{2}\rho^T\rho. \tag{48}$$

Invoking (32), (42), (44), and (46), the time derivative of V_3 yields

$$\begin{aligned}\dot{V}_3 &= \dot{V}_2 + \mathrm{tr}\left\{\tilde{W}^T\Lambda_W^{-1}\dot{\tilde{W}}\right\} + \tilde{D}^T\dot{\tilde{D}} + \rho^T\dot{\rho} \\ &\le -e_1^T k_1 e_1 - e_2^T k_2 e_2 + \left(e_2^T - \rho\right)\left(-\frac{\rho}{\tau} + \bar{Y}\right) \\ &\quad - \tilde{D}^T\left[M_D - \left(\frac{1}{2} + 0.5\Xi\Upsilon^2\right)I_{2\times 2}\right]\tilde{D} \\ &\quad - \sigma_W\mathrm{tr}\left\{\tilde{W}^T\hat{W}\right\} + \frac{1}{2\Xi}\|\tilde{W}\|^2 + \frac{1}{2}\bar{D}^2.\end{aligned} \tag{49}$$

Considering the following facts leads to:

$$-\frac{e_2^T\rho}{\tau} \le \frac{1}{2\tau}e_2^T e_2 + \frac{1}{2\tau}\rho^T\rho \tag{50}$$

$$e_2^T\bar{Y} \le \frac{1}{2}e_2^T e_2 + \frac{1}{2}\bar{Y}^2 \tag{51}$$

$$-\rho\bar{Y} \le \frac{1}{2}\rho^T\rho + \frac{1}{2}\bar{Y}^2 \tag{52}$$

$$-\sigma_W\mathrm{tr}\left\{\tilde{W}^T\hat{W}\right\} \le -\frac{\sigma_W}{2}\|\tilde{W}\|^2 + \frac{\sigma_W}{2}\|W^*\|^2. \tag{53}$$

Substituting (50)–(53) into (49), we obtain

$$\begin{aligned}\dot{V}_3 &\le -e_1^T k_1 e_1 - e_2^T\left[k_2 - \frac{1}{2}\left(\frac{1}{\tau} + I_{2\times 2}\right)\right]e_2 \\ &\quad - \left(\frac{\sigma_W}{2} - \frac{1}{2\Xi}\right)\|\tilde{W}\|^2 - \tilde{D}^T\left[M_D - \frac{1}{2}\left(1 + \Xi\Upsilon^2\right)\right]\tilde{D} \\ &\quad - \rho^T\left[\frac{1}{2}\left(\frac{1}{\tau} + I_{2\times 2}\right)\right]\rho + \frac{\sigma_W}{2}\|W^*\|^2 + \frac{1}{2}\bar{D}^2 + \bar{Y}^2 \\ &\le -aV_3 + C\end{aligned} \tag{54}$$

where

$$\begin{aligned}a = \min\ &\left\{2\lambda_{\min}(k_1), 2\lambda_{\min}\left[k_2 - \frac{1}{2}\left(\frac{1}{\tau} + I_{2\times 2}\right)\right],\right. \\ &\frac{2\left(\frac{\sigma_W}{2} - \frac{1}{2\Xi}\right)}{\lambda_{\max}\left(\Lambda_W{}^{-1}\right)}, 2\lambda_{\min}\left[M_D - \frac{1}{2}\left(1 + \Xi\Upsilon^2\right)\right], \\ &\left.2\lambda_{\min}\left[\frac{1}{2}\left(\frac{1}{\tau} + I_{2\times 2}\right)\right]\right\}\end{aligned} \tag{55}$$

and

$$C = \frac{\sigma_W}{2}\|W^*\|^2 + \frac{1}{2}\bar{D}^2 + \bar{Y}^2. \tag{56}$$

To guarantee $a > 0$, the parameters k_1, k_2, τ, σ_W, Ξ, and M_D are selected as

$$\lambda_{\min}(k_1) > 0, \lambda_{\min}\left[k_2 - \frac{1}{2}\left(\frac{1}{\tau} + I_{2\times 2}\right)\right] > 0$$
$$\left(\frac{\sigma_W}{2} - \frac{1}{2\Xi}\right) > 0, \lambda_{\min}\left[M_D - \frac{1}{2}\left(1 + \Xi\Upsilon^2\right)\right] > 0$$
$$\lambda_{\min}\left[\frac{1}{2}\left(\frac{1}{\tau} + I_{2\times 2}\right)\right] > 0. \tag{57}$$

Theorem 1: Considering the 2-DOF helicopter system described in (3)–(5) with input saturation, external disturbances, and output constraints, the barrier function is given as (18), the nonlinear DO are designed as (25) and (26), and the updating law is proposed as (46). Under the adaptive NN control law (45), the signals of the closed-loop system are semiglobally uniformly bounded. Moreover, the error signals e_1, e_2, $\tilde{W}$, $\tilde{D}$, and ρ will converge into the compact sets Ω_{e_1}, Ω_{e_2}, $\Omega_{\tilde{W}}$, $\Omega_{\tilde{D}}$, and Ω_ρ, respectively, defined by

$$\Omega_{e_1} = \left\{e_1 \in \mathbb{R}^2 | \|e_1\| \le \sqrt{N}\right\} \tag{58}$$
$$\Omega_{e_1} = \left\{e_2 \in \mathbb{R}^2 | \|e_2\| \le \sqrt{N}\right\} \tag{59}$$
$$\Omega_{\tilde{W}} = \left\{\tilde{W} \in \mathbb{R}^{j\times 2} | \left\|\tilde{W}\right\| \le \sqrt{\frac{N}{\lambda_{\min}\left(\Lambda_W^{-1}\right)}}\right\} \tag{60}$$
$$\Omega_{\tilde{D}} = \left\{\tilde{D} \in \mathbb{R}^2 | \left\|\tilde{D}\right\| \le \sqrt{N}\right\} \tag{61}$$
$$\Omega_{\tilde{\rho}} = \left\{\tilde{\rho} \in \mathbb{R}^2 | \|\tilde{\rho}\| \le \sqrt{N}\right\} \tag{62}$$

where $N = 2(V_3(0) + (C/a))$, and a and C are two positive constants.

Proof: Multiplying both sides of (54) by e^{at} yields

$$\frac{d}{dt}\left(V_3 e^{at}\right) \le Ce^{at}. \tag{63}$$

Integrating (63), we have

$$V_3 \le \left(V_3(0) - \frac{C}{a}\right)e^{-at} + \frac{C}{a} \le V_3(0) + \frac{C}{a}. \tag{64}$$

For convenience of analysis, we define $N = 2(V_3(0) + (C/a))$. Invoking (48), we derive

$$e_1^T e_1 \le N, e_2^T e_2 \le N, \mathrm{tr}\left\{\tilde{W}\Lambda_W^{-1}\tilde{W}\right\} \le N,$$
$$\tilde{D}^T\tilde{D} \le N, \tilde{\rho}^T\tilde{\rho} \le N. \tag{65}$$

Then

$$\|e_1\| \le \sqrt{N}, \|e_2\| \le \sqrt{N}, \left\|\tilde{W}\right\| \le \sqrt{\frac{N}{\lambda_{\min}\left(\Lambda_W^{-1}\right)}}$$
$$\left\|\tilde{D}\right\| \le \sqrt{N}, \|\tilde{\rho}\| \le \sqrt{N}. \tag{66}$$

Therefore, the proof is completed.

IV. Numerical Simulation and Comparisons

To confirm the validity of the proposed control, we conduct three sets of numerical simulations to study the trajectory tracking problem of a 2-DOF helicopter system. First, we impose the output constraints to a prescribed time period based on different values of T_x and T_y, aiming to verify the effectiveness of the proposed control in addressing the OCIPT issue. Subsequently, the proposed control is compared with a control method that approximates uncertainty using fuzzy logic systems (FLSs) to verify its feasibility. Finally, to further validate the superiority of the proposed control, it is compared with the simulation results of the ATVBLF presented in [33].

In the presented simulation, the system's parameters are set as follows: $T_{pp} = 0.0215$ kg $\cdot$ m^2, $T_{yy} = 0.0237$ kg $\cdot$ m^2, $l_a = 0.0025$ m, $m_v = 1.0750$ kg, $D_{pp} = 0.0071$ N/V, $D_{yy} = 0.0220$ N/V, $L_{ff} = 0.0011$ N $\cdot$ m/V, $L_{fd} = 0.0021$ N $\cdot$ m/V, $L_{df} = -0.0027$ N $\cdot$ m/V, and $L_{dd} = 0.0022$ N $\cdot$ m/V. Moreover, the desired trajectory is given by $x_d = [0.5(\tanh(5(t - T_x)) + \tanh(5(t - T_y)))\sin(t) + 0.3\cos(t), 0.5(\tanh(5(t - T_x)) + \tanh(5(t - T_y)))\cos(t) + 0.3\sin(t)]^T$, and the external disturbance is defined as $[-0.2\sin(0.6t + 0.4), -0.2\sin(0.6t + 0.2) + 0.1\cos(0.4t)]^T$.

For the proposed adaptive NN control, the variance is chosen as 16, the initial weights are set as $\hat{W}(0) = 0$, and 2^5 nodes are allocated for each $H_j(X)$, with centers selected from the range of $[-1, 1] \times [-1, 1] \times [-1, 1] \times [-1, 1] \times [-1, 1] \times [-1, 1] \times [-1, 1] \times [-1, 1]$. Furthermore, the control parameters are set as $\Lambda_W = 15I_{32\times 32}$ and $\sigma_W = 2$. The other parameters are selected as $\tau = 0.01$ and $\Xi = 1$. The design matrix of the DO is set as $M_D =$ diag$[10, 8]$. The upper and lower bounds of the saturation are chosen as $u_{\max} = 24$V and $u_{\min} = -24$V, respectively.

A. Proposed Control With Different Values of T_x and T_y

1) Case 1: We set $T_x = 10$ and $T_y = 30$, implying that output constraints are imposed between 10 and 30 s after the system runs for a period, with no constraints at other times. In addition, the initial system's conditions are $x_1 = [0.3, -0.8]^T$ and $x_2 = [0, 0]^T$. The control parameters are designed as $k_1 =$ diag$[15, 15]$, $k_2 =$ diag$[15, 15]$, and $\mu_1 = \mu_2 = 0.7$. The constraint boundaries of the system error are $Q_{f1} = Q_{f2} = 0.08 + 0.02\sin(t)$ and $Q_{g1} = Q_{g2} = 0.09 + 0.025\sin(t)$, and the upper and lower boundaries of the state variable are $E_{F1} = E_{F2} = 0.4 + 0.02\sin(t)$ and $E_{G1} = E_{G2} = -0.41 - 0.025\sin(t)$ respectively.

The simulation results are shown in Fig. 3. The responses of Θ and Ψ are shown in Fig. 3(a) and (b) respectively. As expected, the system satisfies constraints within the prescribed period of 10–30 s, being restricted between state boundaries E_{F1} and E_{G1}, while there are no constraints during the other periods 0–10 s and 30–50 s. It is evident from the tracking errors in Fig. 3(c) and (d) that the errors e_{11} and e_{12} are bounded, and the system can quickly track the desired trajectory. Furthermore, Fig. 3(e) and (f) illustrates the control input voltage and input saturation voltage, respectively. It can be concluded that this control method can still achieve

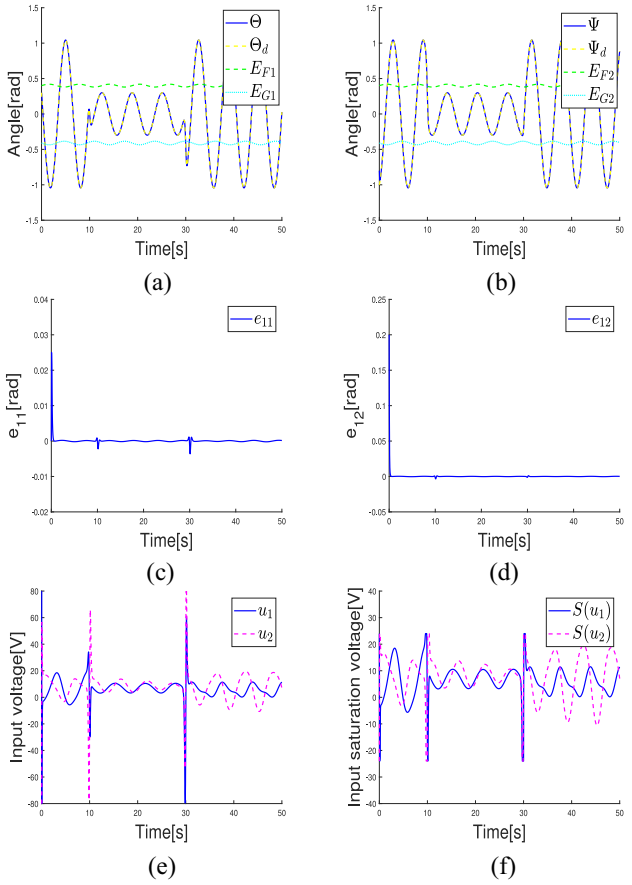

Fig. 3. Control performance for case 1. (a) Tracking response of Θ. (b) Tracking response of Ψ. (c) Trajectory of e_{11}. (d) Trajectory of e_{12}. (e) Input voltages u_1 and u_2. (f) Input saturation voltages $S(u_1)$ and $S(u_2)$.

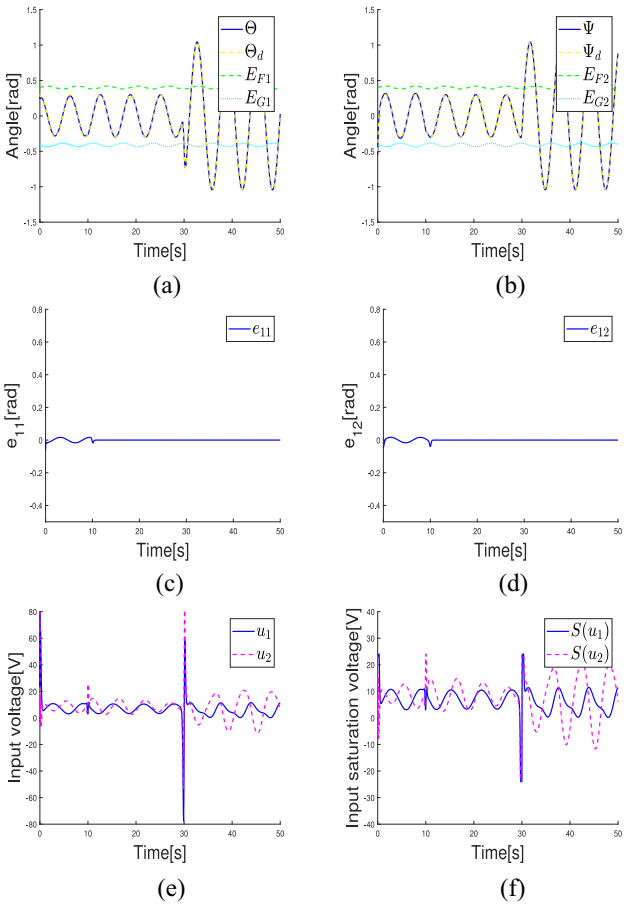

Fig. 4. Control performance for case 2. (a) Tracking response of Θ. (b) Tracking response of Ψ. (c) Trajectory of e_{11}. (d) Trajectory of e_{12}. (e) Input voltages u_1 and u_2. (f) Input saturation voltages $S(u_1)$ and $S(u_2)$.

excellent control performance even when subjected to saturation conditions.

2) Case 2: We set $T_x = 0$ and $T_y = 30$, indicating that the output constraints are imposed on the system during the initial 0–30 s, after which these constraints are lifted. In addition, the initial system's conditions are $x_1 = [0.24, -0.55]^T$ and $x_2 = [0, 0]^T$. The control parameters are presented as $k_1 = \text{diag}[60, 60]$, $k_2 = \text{diag}[60, 60]$, and $\mu_1 = \mu_2 = 0.7$. The constraint boundaries are the same as case 1.

The responses of the system are depicted in Fig. 4, where Fig. 4(a) and (b) illustrates the evolution of attitude angles tracking. As expected, the system conforms to constraints in the prescribed 0–30 s, confined within the state boundaries of E_{F1} and E_{G1}. Once the system reaches the 30 s mark, the constraints are removed. Fig. 4(c) and (d) depicts the tracking error of the attitude angles, suggesting that the errors are bounded and convergent to a small range centered around zero in a short period. Fig. 4(e) and (f) shows the input voltage and input saturation voltage, respectively, concluding that the system maintains good control effectiveness even under saturation conditions.

3) Case 3: We set $T_x = 0$ and $T_y = 0$, meaning that the system remains free from output constraints for all $t \geq 0$. In addition, the initial system's conditions are $x_1 = [0.35, 0.07]^T$ and $x_2 = [0, 0]^T$. The control parameters are presented as $k_1 = \text{diag}[40, 40]$, $k_2 = \text{diag}[50, 50]$, and $\mu_1 = \mu_2 = 0.03$. The constraint boundaries are the same as case 1.

The system's dynamical responses are illustrated in Fig. 5. Fig. 5(a) and (b) depicts the tracking performance for Θ and Ψ, respectively. As anticipated, the system is unbounded for all $t \geq 0$. An analysis of the evolution of errors depicted in Fig. 5(c) and (d) indicates that the errors remain bounded and eventually approach zero. Fig. 5(e) and (f) shows the input voltage and input saturation voltage, respectively, and it can be concluded that the system can still maintain satisfactory control effect under saturation conditions.

Through the simulation results presented above, we can observe that the proposed control enables a smooth transition of the system between unrestricted and restricted phases. Simultaneously, the proposed method successfully expanded multiple applications (such as cases 1–3) under a unified control framework by adjusting T_x, T_y, and associated parameters, effectively solving the OCIPT problem. In addition, it also ensures satisfactory tracking control and input performance, thereby verifying the feasibility of the proposed control.

B. Comparison of the Proposed Control and FLS

To validate the feasibility of the proposed control, we compare the simulation results of case 1 with those obtained

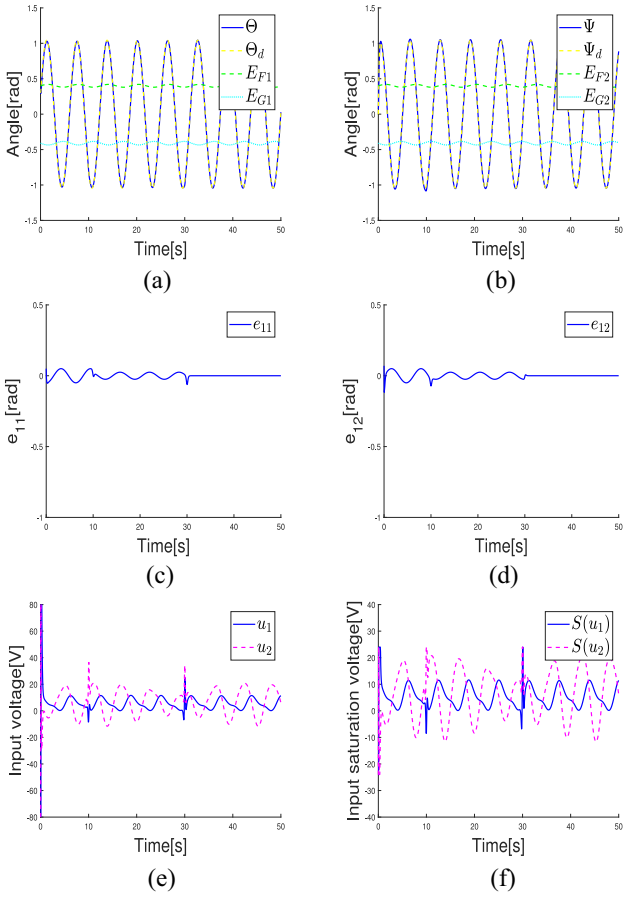

Fig. 5. Control performance for case 3. (a) Tracking response of Θ. (b) Tracking response of Ψ. (c) Trajectory of e_{11}. (d) Trajectory of e_{12}. (e) Input voltages u_1 and u_2. (f) Input saturation voltages $S(u_1)$ and $S(u_2)$.

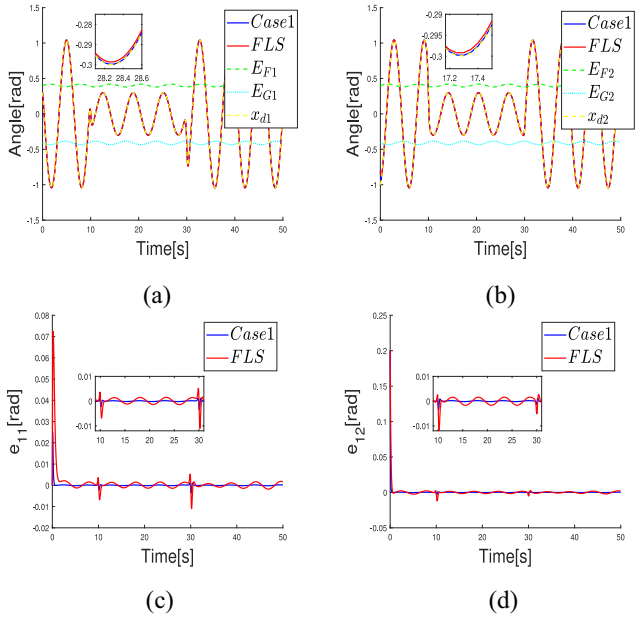

Fig. 6. Comparative results between the case 1 and FLS. (a) Tracking response of Θ. (b) Tracking response of Ψ. (c) Trajectory of e_{11}. (d) Trajectory of e_{12}.

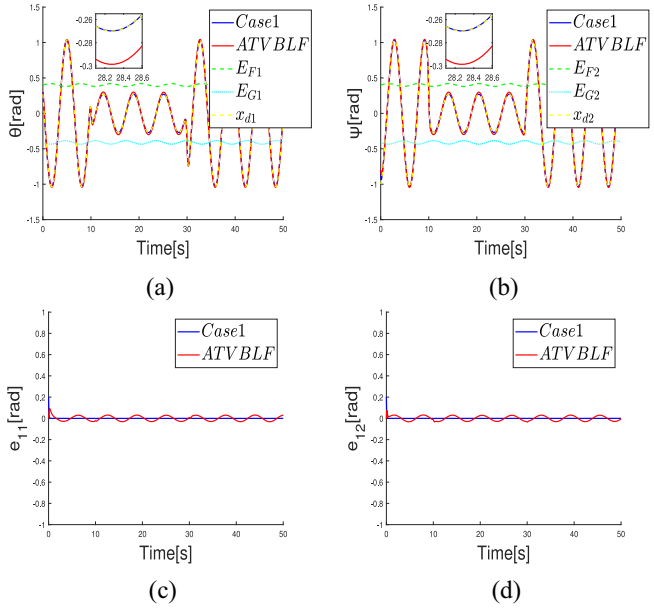

Fig. 7. Comparative results between the case 1 and ATVBLF. (a) Tracking response of Θ. (b) Tracking response of Ψ. (c) Trajectory of e_{11}. (d) Trajectory of e_{12}.

using FLS. For ease of comparison, this control employs the same design parameters as those used in case 1. The simulation results are illustrated in Fig. 6. Fig. 6(a) and (b) depicts the tracking performance of Θ and Ψ, respectively. Evidently, the proposed control method can track the desired trajectory better than the FLS. Fig. 6(c) and (d) represents the trajectory errors e_{11} and e_{12}. The results demonstrate that the proposed method can consistently achieve smaller errors compared to the FLS. Therefore, compared with the FLS, the proposed control can better track the expected trajectory.

C. Comparison of the Proposed Control and the ATVBLF

To verify the superiority of the proposed control method, it is compared with the control method using the ATVBLF. For consistency, the same design parameters as in case 1 are used. The simulation results are presented in Fig. 7. Fig. 7(a) and (b) illustrates the tracking performance of Θ and Ψ, respectively. The proposed control method demonstrates more satisfactory tracking performance. Fig. 7(c) and (d) shows the trajectory errors e_{11} and e_{12}. The results indicate that, compared to the ATVBLF, the proposed control achieves faster convergence of the tracking error to a very small range and exhibits smaller oscillations in the trajectory error. This strongly validates the superiority of the proposed control.

V. Conclusion

In this study, an adaptive NN control was proposed for a 2-DOF helicopter system with input saturation, external disturbances, and output constraints. First, an RBFNN was used to estimate uncertainties within the helicopter system. In addition, a DO was used to mitigate the adverse effects of unknown compound disturbances, including errors in NN estimation, input saturation, and external disturbances. To address the OCIPT problem, a new time-shifted function and an adjusted barrier functions were introduced. Subsequently,

Lyapunov function stability analysis was used to ensure the stable performance of the closed-loop system. Finally, the effectiveness of the proposed adaptive NN control was validated through simulation results. In the future, we will delve deeper into the input delay and state constraint issues present in actual helicopter operations, aiming to enhance flight control performance.

REFERENCES

[1] L. Qian and H. H. Liu, "Path-following control of a quadrotor UAV with a cable-suspended payload under wind disturbances," *IEEE Trans. Ind. Electron.*, vol. 67, no. 3, pp. 2021–2029, Mar. 2020.

[2] V. K. Singh and S. Kamal, "Prescribed-time adaptive backstepping control of an uncertain nonlinear 2-DOF helicopter," *IEEE Trans. Circuits Syst. II, Exp. Briefs*, vol. 70, no. 11, pp. 4138–4142, Nov. 2023.

[3] S. Wang, "Approximation-free control for nonlinear helicopters with unknown dynamics," *IEEE Trans. Circuits Syst. II, Exp. Briefs*, vol. 69, no. 7, pp. 3254–3258, Jul. 2022.

[4] C. Wang, X. Huo, K. Ma, and R. Ji, "PID-like model free adaptive control with discrete extended state observer and its application on an unmanned helicopter," *IEEE Trans. Ind. Informat.*, vol. 19, no. 11, pp. 11265–11274, Nov. 2023.

[5] Y.-C. Lai and T.-Q. Le, "Adaptive learning-based observer with dynamic inversion for the autonomous flight of an unmanned helicopter," *IEEE Trans. Aerosp. Electron. Syst.*, vol. 57, no. 3, pp. 1803–1814, Jun. 2021.

[6] L. Dutta and D. Kumar Das, "Adaptive model predictive control design using multiple model second level adaptation for parameter estimation of two-degree freedom of helicopter model," *Int. J. Robust Nonlinear Control*, vol. 31, no. 8, pp. 3248–3278, 2021.

[7] T. Y. Chun, J. B. Park, and Y. H. Choi, "Reinforcement q-learning based on multirate generalized policy iteration and its application to a 2-DOF helicopter," *Int. J. Control, Autom. Syst.*, vol. 16, pp. 377–386, Feb. 2018.

[8] R. Maiti, K. D. Sharma, and G. Sarkar, "PSO based parameter estimation and PID controller tuning for 2-DOF nonlinear twin rotor MIMO system," *Int. J. Autom. Control*, vol. 12, no. 4, pp. 582–609, 2018.

[9] B. Luo, H.-N. Wu, and T. Huang, "Optimal output regulation for model-free quanser helicopter with multistep Q-learning," *IEEE Trans. Ind. Electron.*, vol. 65, no. 6, pp. 4953–4961, Jun. 2018.

[10] P. John-Baptiste, J. T. Johnson, and G. E. Smith, "Neural network-based control of an adaptive radar," *IEEE Trans. Aerosp. Electron. Syst.*, vol. 58, no. 1, pp. 168–179, Feb. 2022.

[11] H. Zhang, Y. Zhou, and Z. Zeng, "Master-slave synchronization of neural networks with unbounded delays via adaptive method," *IEEE Trans. Cybern.*, vol. 53, no. 5, pp. 3277–3287, May 2023.

[12] H. Zhang and Z. Zeng, "Synchronization of nonidentical neural networks with unknown parameters and diffusion effects via robust adaptive control techniques," *IEEE Trans. Cybern.*, vol. 51, no. 2, pp. 660–672, Feb. 2021.

[13] T. Zhang, X. Wang, X. Xu, and C. L. P. Chen, "GCB-Net: Graph convolutional broad network and its application in emotion recognition," *IEEE Transa. Affect. Comput.*, vol. 13, no. 1, pp. 379–388, Jan.–Mar. 2022.

[14] X. Yang and X. Zheng, "Adaptive NN backstepping control design for a 3-DOF helicopter: Theory and experiments," *IEEE Trans. Ind. Electron.*, vol. 67, no. 5, pp. 3967–3979, May 2020.

[15] Z. Zhao, W. He, T. Zou, T. Zhang, and C. L. P. Chen, "Adaptive broad learning neural network for fault-tolerant control of 2-DOF helicopter systems," *IEEE Trans. Syst., Man, Cybern., Syst.*, vol. 53, no. 12, pp. 7560–7570, Dec. 2023.

[16] Z. Zhao, J. Zhang, S. Chen, W. He, and K.-S. Hong, "Neural-network-based adaptive finite-time control for a two-degree-of-freedom helicopter system with an event-triggering mechanism," *IEEE/CAA J. Automatica Sinica*, vol. 10, no. 8, pp. 1754–1765, Aug. 2023.

[17] T. Zou, H. Wu, W. Sun, and Z. Zhao, "Adaptive neural network sliding mode control of a nonlinear two-degrees-of-freedom helicopter system," *Asian J. Control*, vol. 25, no. 3, pp. 2085–2094, 2023.

[18] W. Bai, Q. Zhou, T. Li, and H. Li, "Adaptive reinforcement learning neural network control for uncertain nonlinear system with input saturation," *IEEE Trans. Cybern.*, vol. 50, no. 8, pp. 3433–3443, Aug. 2020.

[19] J. Yu, P. Shi, C. Lin, and H. Yu, "Adaptive neural command filtering control for nonlinear MIMO systems with saturation input and unknown control direction," *IEEE Trans. Cybern.*, vol. 50, no. 6, pp. 2536–2545, Jun. 2020.

[20] Z. Song, P. Li, Z. Wang, X. Huang, and W. Liu, "Adaptive tracking control for switched uncertain nonlinear systems with input saturation and unmodeled dynamics," *IEEE Trans. Circuits Syst. II, Exp. Briefs*, vol. 67, no. 12, pp. 3152–3156, Dec. 2020.

[21] Z. Ma and P. Huang, "Adaptive neural-network controller for an uncertain rigid manipulator with input saturation and full-order state constraint," *IEEE Trans. Cybern.*, vol. 52, no. 5, pp. 2907–2915, May 2022.

[22] W. Sun, S. Diao, S.-F. Su, and Z.-Y. Sun, "Fixed-time adaptive neural network control for nonlinear systems with input saturation," *IEEE Trans. Neural Netw. Learn. Syst.*, vol. 34, no. 4, pp. 1911–1920, Apr. 2023.

[23] M. Lv, W. Yu, and S. Baldi, "The set-invariance paradigm in fuzzy adaptive DSC design of large-scale nonlinear input-constrained systems," *IEEE Trans. Syst., Man, Cybern., Syst.*, vol. 51, no. 2, pp. 1035–1045, Feb. 2021.

[24] G. Li, X. Chen, J. Yu, and J. Liu, "Adaptive neural network-based finite-time impedance control of constrained robotic manipulators with disturbance observer," *IEEE Trans. Circuits Syst. II, Exp. Briefs*, vol. 69, no. 3, pp. 1412–1416, Mar. 2022.

[25] Q. Zhang and D. He, "Disturbance-observer-based adaptive fuzzy control for strict-feedback switched nonlinear systems with input delay," *IEEE Trans. Fuzzy Syst.*, vol. 29, no. 7, pp. 1942–1952, Jul. 2021.

[26] S. Shao and M. Chen, "Adaptive neural discrete-time fractional-order control for a UAV system with prescribed performance using disturbance observer," *IEEE Trans. Syst., Man, Cybern., Syst.*, vol. 51, no. 2, pp. 742–754, Feb. 2021.

[27] M. Li and Y. Chen, "Robust adaptive sliding mode control for switched networked control systems with disturbance and faults," *IEEE Trans. Ind. Informat.*, vol. 15, no. 1, pp. 193–204, Jan. 2019.

[28] R. Zhang, B. Xu, and P. Shi, "Output feedback control of micromechanical gyroscopes using neural networks and disturbance observer," *IEEE Trans. Neural Netw. Learn. Syst.*, vol. 33, no. 3, pp. 962–972, Mar. 2022.

[29] J. Ni and P. Shi, "Global predefined time and accuracy adaptive neural network control for uncertain strict-feedback systems with output constraint and dead zone," *IEEE Trans. Syst., Man, Cybern., Syst.*, vol. 51, no. 12, pp. 7903–7918, Dec. 2021.

[30] R. Meng, C. Hua, K. Li, and P. Ning, "A multifilters approach to adaptive event-triggered control of uncertain nonlinear systems with global output constraint," *IEEE Trans. Cybern.*, vol. 54, no. 2, pp. 1143–1153, Feb. 2024.

[31] S. Dong, K. Liu, M. Liu, G. Chen, and T. Huang, "Adaptive neural network-quantized tracking control of uncertain unmanned surface vehicles with output constraints," *IEEE Trans. Intell. Veh.*, vol. 9, no. 2, pp. 3293–3304, Feb. 2024, doi: 10.1109/TIV.2023.3331905.

[32] S. Yan, L. Shi, H. Zhang, S. Yao, and Y. Zhou, "Safety-critical model-free adaptive iterative learning control for multi-agent consensus using control barrier functions," *IEEE Trans. Circuits Syst. II, Exp. Briefs*, vol. 71, no. 1, pp. 221–225, Jan. 2024.

[33] Y.-J. Liu, L. Ma, L. Liu, S. Tong, and C. L. P. Chen, "Adaptive neural network learning controller design for a class of nonlinear systems with time-varying state constraints," *IEEE Trans. Neural Netw. Learn. Syst.*, vol. 31, no. 1, pp. 66–75, Jan. 2020 doi: 10.1109/TNNLS.2019.2899589,

[34] S. Farzan, V. Azimi, A.-P. Hu, and J. Rogers, "Adaptive control of wire-borne underactuated brachiating robots using control Lyapunov and barrier functions," *IEEE Trans. Control Syst. Technol.*, vol. 30, no. 6, pp. 2598–2614, Nov. 2022.

[35] S.-K. Kim, K. S. Kim, and C. K. Ahn, "Order reduction approach to velocity sensorless performance recovery pd-type attitude stabilizer for 2-DOF helicopter applications," *IEEE Trans. Ind. Informat.*, vol. 18, no. 10, pp. 6848–6856, Oct. 2022.

[36] N. Zerari, M. Chemachema, and N. Essounbouli, "Neural network based adaptive tracking control for a class of pure feedback nonlinear systems with input saturation," *IEEE/CAA J. Automatica Sinica*, vol. 6, no. 1, pp. 278–290, Jan. 2019.

[37] M. Chen, H. Ma, Y. Kang, and Q. Wu, "Adaptive neural safe tracking control design for a class of uncertain nonlinear systems with output constraints and disturbances," *IEEE Trans. Cybern.*, vol. 52, no. 11, pp. 12571–12582, Nov. 2022.

[38] S. Sui, C. L. P. Chen, and S. Tong, "A novel adaptive NN prescribed performance control for stochastic nonlinear systems," *IEEE Trans. Neural Netw. Learn. Syst.*, vol. 32, no. 7, pp. 3196–3205, Jul. 2021.

[39] W. He, L. Kong, Y. Dong, Y. Yu, C. Yang, and C. Sun, "Fuzzy tracking control for a class of uncertain MIMO nonlinear systems with state constraints," *IEEE Trans. Syst., Man, Cybern., Syst.*, vol. 49, no. 3, pp. 543–554, Mar. 2019.
[40] J. Qiu, K. Sun, T. Wang, and H. Gao, "Observer-based fuzzy adaptive event-triggered control for pure-feedback nonlinear systems with prescribed performance," *IEEE Trans. Fuzzy Syst.*, vol. 27, no. 11, pp. 2152–2162, Nov. 2019.
[41] H. Li, Y. Wu, and M. Chen, "Adaptive fault-tolerant tracking control for discrete-time multiagent systems via reinforcement learning algorithm," *IEEE Trans. Cybern.*, vol. 51, no. 3, pp. 1163–1174, Mar. 2021.
[42] L. Kong, W. He, Z. Liu, X. Yu, and C. Silvestre, "Adaptive tracking control with global performance for output-constrained MIMO nonlinear systems," *IEEE Trans. Autom. Control*, vol. 68, no. 6, pp. 3760–3767, Jun. 2023.
[43] Z. Li, C.-Y. Su, L. Wang, Z. Chen, and T. Chai, "Nonlinear disturbance observer-based control design for a robotic exoskeleton incorporating fuzzy approximation," *IEEE Trans. Ind. Electron.*, vol. 62, no. 9, pp. 5763–5775, Sep. 2015.
[44] Y.-J. Liu, Q. Zeng, L. Liu, and S. Tong, "An adaptive neural network controller for active suspension systems with hydraulic actuator," *IEEE Trans. Syst., Man, Cybern., Syst.*, vol. 50, no. 12, pp. 5351–5360, Dec. 2020.

Zhijia Zhao (Senior Member, IEEE) received the B.Eng. degree in automatic control from the North China University of Water Resources and Electric Power, Zhengzhou, China, in 2010, and the M.Eng. and Ph.D. degrees in automatic control from the South China University of Technology, Guangzhou, China, in 2013 and 2017, respectively.

He is currently a Professor with the School of Mechanical and Electrical Engineering, Guangzhou University, Guangzhou. His research interests include adaptive and learning control, flexible mechanical systems, and robotics.

Di Zhang received the B.Eng. degree in robotics engineering from Guangzhou University, Guangzhou, China, in 2022, where he is currently pursuing the M.Eng. degree.

His research interests include adaptive control, intelligent control, and robotics.

Jiale Wu received the B.Eng. degree in mechanical manufacturing and automation from Guangdong Ocean University, Zhanjiang, China, in 2021. He is currently pursuing the M.Eng. degree in mechanical manufacturing and automation from Guangzhou University, Guangzhou, China, in 2024.

His research interests include adaptive control, intelligent control, and robotics.

Zhijie Liu (Member, IEEE) received the B.Sc. degree in electrical engineering and automation from the China University of Mining and Technology Beijing, Beijing, China, in 2014, and the Ph.D. degree in control theory control and control engineering from Beihang University, Beijing, in 2019.

In 2017, he was a Research Assistant with the Department of Electrical Engineering, University of Notre Dame, Notre Dame, IN, USA, for twelve months. He is currently a Full Professor with the School of Intelligence Science and Technology, University of Science and Technology Beijing, Beijing. His research interests include adaptive control, modeling and vibration control for flexible structures.

Min Wang (Member, IEEE) received the B.Sc. degree in mathematics and the M.Sc. degree in applied mathematics from Bohai University, Jinzhou, China, in 2003 and 2006, respectively, and the Ph.D. degree in system theory from Qingdao University, Qingdao, China, in 2009.

She was a Visiting scholar with the Department of Computer Science, Brunel University London, London, U.K., from 2017 to 2018. She is currently a Professor with the School of Automation Science and Engineering, South China University of Technology, Guangzhou, China. She has authored or co-authored over 40 papers published in international journals. Her current research interests include intelligent control, dynamic learning, robot control, and event-triggered control.

Prof. Wang is an Associate Editor of three international journals, including *International Journal of Systems Science*, IEEE ACCESS, and *Control Theory and Applications*.

Keum-Shik Hong (Life Fellow, IEEE) received the B.S. degree in mechanical design from Seoul National University, Seoul, South Korea, in 1979, the M.S. degree in mechanical engineering from Columbia University, New York, NY, USA, in 1987, and the M.S. degree in applied mathematics and the Ph.D. degree in mechanical engineering from the University of Illinois at Urbana–Champaign, Champaign, IL, USA, in 1991.

He joined the School of Mechanical Engineering, Pusan National University, Busan, South Korea, in 1993. His research interests include brain–computer interface, nonlinear systems theory, adaptive control, and distributed parameter systems.

Dr. Hong has received many awards, including the Best Paper Award from the KFSTS of Korea in 1999, and the Presidential Award of Korea in 2007. He served as an Associate Editor for *Automatica* from 2000 to 2006, as an Editor-in-Chief for the *Journal of Mechanical Science and Technology* from 2008 to 2011, and is serving as an Editor-in-Chief for the *International Journal of Control, Automation, and Systems*. He was a Past President of the Institute of Control, Robotics and Systems, Korea, and is a President of the Asian Control Association. He is a Fellow of the Korean Academy of Science and Technology, an ICROS Fellow, and a member of the National Academy of Engineering of Korea.